Statistical analysis of the variability of reactive trace gases (SO2, NO2 and ozone) in Greater Cairo during dust storm events

Mohamed Boraiy, Mossad El-Metwally, Ali Wheida, Mostafa El-Nazer, Salwa Hassan, Fatma El-Sanabary, Stéphane Alfaro, Magdy Abdelwahab, Agnès Borbon

Journal of Atmospheric Chemistry
https://doi.org/10.1007/s10874-023-09449-4

Statistical analysis of the variability of reactive trace gases (SO_2, NO_2 and ozone) in Greater Cairo during dust storm events

Mohamed Boraiy[1] · Mossad El-Metwally[2] · Ali Wheida[3] · Mostafa El-Nazer[3] · Salwa K. Hassan[4] · Fatma F. El-Sanabary[1] · Stéphane C. Alfaro[5] · Magdy Abdelwahab[6] · Agnès Borbon[7]

Received: 28 March 2023 / Accepted: 20 June 2023

Abstract
The data of 17 air quality monitoring stations of Greater Cairo are used to perform a statistical analysis aiming to detect any heterogeneous surface effects of mineral dust on the distribution of reactive trace gases (SO_2 NO_2, and ozone) in. After a thorough quality check, the methodology consisted of i) selecting representative stations by agglomerative hierarchical clustering, ii) identifying dust events based on PM_{10} measurements, remote sensing observations, and meteorology, and iii) applying the non-parametric Kruskal Wallis (KW) hypothesis test to compare (at the 95% confidence level) trace gas concentrations during dust and non-dust events. The representative stations display either a background-like or a bimodal variability with concentrations (even that of the secondary product NO_2) peaking at traffic rush hours but during dust storms all stations capture the signal of mineral dust advection. Eight wintertime and springtime dust cases are retained for the study. After the role of the confounding factors (i.e., ventilation index, relative humidity, and photolysis) has been carefully discussed and taken into account, the KW test shows that there is no significant reduction of the SO_2, NO_2 and ozone concentrations attributable to dust during 7 of the 8 events. The drop of the concentrations coinciding with the advection of dry dust-laden Saharan air masses is rather an effect of the dilution resulting from the combination of large wind speed and mixing layer height than of the heterogeneous uptake of these gases on the mineral dust surface.

Keywords Mineral dust · Heterogeneous uptake · Hierarchical analysis · Greater Cairo · Air quality · Trace gas variability

1 Introduction

Heterogeneous reactions with cloud droplets and aerosols are found to be important for atmospheric chemistry. Since the seminal work of (Dentener et al. 1996), special emphasis has been given to reactions on mineral dust aerosols because these particles provide a large surface area for heterogeneous reactions in the troposphere. Indeed, mineral aerosols

Extended author information available on the last page of the article

produced from windblown soils are an important component of the earth-atmosphere system which is estimated to be between 1000 to 3000 Tg emitted annually (Usher et al. 2003). Convincing evidence that heterogeneous chemistry on mineral dust significantly alters the concentration of important atmospheric gases has been first established by model settings and laboratory experiments. For instance, the heterogeneous chemistry occurring on dust particles acted as a sink reducing ozone (O_3) by up to 9 % and sulfur dioxide (SO_2) by up to 27 % in an Asian dust storm travelling over the Pacific (Wang et al. 2012). It has also been found that heterogeneous chemistry, including that of SO_2 and NOx on dust, plays a significant role in regional haze formation in China (He et al. 2014). However, the magnitude of the uptake simulated by the models is still uncertain because it depends on various environmental conditions and on the uptake coefficient (γ) derived from laboratory experiments. Indeed, the uncertainties in γ are very large as they can cover more than three orders of magnitude for certain species (Zhang and Carmichael 1999; Bian and Zender 2003). For example, some studies have reported values ranging from 2.0×10^{-6} to 2.5×10^{-3} for O_3 and from 2.0×10^{-6} to 1.6×10^{-2} for HNO_3 (Goodman et al. 2000; Underwood et al. 2001; Michel et al. 2002). In their coated-wall flow tube experiments performed with a variety of Saharan dust samples, Ndour et al. (2008) highlighted the effect of light on the photochemical uptake of NO_2: as compared to dark conditions, this uptake could be multiplied by a factor of 8 to 15 depending on the source region. Zhang et al. (2019) also showed that the uptake is greatly enhanced by small amount of surface-adsorbed water because of the exponential relationship between SO_2 and Relative Humidity (RH). Finally, there is also evidence of a synergistic effect when various trace gas species coexist like NOx with SO_2 (He et al. 2014) or NO_2 and ammonia (NH_3) (Zhang et al. 2019). All these laboratory studies suggest that dust storms could have the potential to change the distribution of reactive trace gases in the troposphere but there is still a need to evaluate the real-life impact of natural dust on atmospheric processes.

Xie et al. (2005) explored at three sampling sites in Beijing (China) the changes in reactive trace gases before, during, and after a dust storm. To our knowledge, no other urban scale study has evaluated those effects from an in-situ field perspective especially in the megacities of Africa and the Middle East where mineral dust is present and where anthropogenic emissions are expected to increase dramatically in the next century (Thera et al. 2022; Salameh et al. 2017; Knippertz et al. 2015). Greater Cairo (GC), is a good example of these megacities. It consists of three different districts (Cairo, Giza, and Kalubia), its population approaches 22 million and hosts more than one- third of the total industrial activity of Egypt (Hereher et al. 2021). As a consequence, GC suffers from high mass concentration of atmospheric pollutants such as airborne particulate matter (PM), carbon monoxide (CO), nitrogen oxides (NOx), ozone (O_3) , sulfur dioxide (SO_2) and organic compounds (OC) (Abu- Allaban et al. 2002, 2009; Hassan 2018a, b, c; Marchetti et al. 2019; Shaltout et al. 2020; El-Dars et al. 2004; Talaat et al. 2021). The origin of PM is both natural (desert dust) and anthropogenic (traffic, industry, biomass and waste burning) (Abu-Allaban et al. 2007; El-Metwally et al. 2011; Favez et al. 2008a, b; Mahmoud et al. 2008; Shaltout et al. 2018a, 2019). In their recent analysis of the spatial and temporal variability of the PM_{10}, SO_2, NO_2, CO and O_3 mass concentrations at the 17 sites of this study, Mostafa et al. (2019) suggested that biomass burning (sulfur-containing fuels) by industry and transportation sectors is the main source of SO_2 and NO_2. Being located downwind of the Saharan Desert, GC also experiences regularly high dust loadings (Hassan and Khoder 2017; Eltahan et al. 2018; Hassan 2018b; Shaltout et al. 2018b), which makes it a perfect place for studying the potential interactions between pollution and mineral dust.

In this work, we propose to use a statistical approach based on in-situ observations to detect any effect of reactive trace gas (SO_2, NO_2, and ozone) uptake by mineral dust at an urban scale. A multi-pollutant and multi-year database of gaseous (NO_2, SO_2, O_3) and particulate (PM_{10}) concentrations measured in the Greater Cairo area has been collected and quality-checked in combination with the meteorological measurements of the Egyptian Meteorological Authority (EMA). The objective was to analyze the spatial and temporal variability of trace gases during dust events with the underlying question: are we able to evidence any impact (surface uptake) of the presence of dust on the ozone, NO_2, and SO_2 concentrations?

2 Data and methods

The methodology consists of i) a quality check and selection of the air quality data between 2010 and 2014, ii) extracting representative stations by agglomerative hierarchical clustering, ii) isolating dust events on the basis of PM_{10} in-situ measurements, remote sensing (sunphotometer and satellite) observations, and air mass back-trajectory analysis, and iv) applying a non-parametric hypothesis test (the Kruskal Wallis – KW test) to compare trace gas concentrations during dust and non-dust events. In the following we will first describe the data before detailing the methodology.

2.1 In-situ observations and clustering of the ground stations

The in-situ air quality observations are performed at the ground stations of the Egyptian Environmental Affairs Agency (EEAA) and Egyptian Meteorological Authority (EMA). The Air Quality Network data include the hourly mass concentrations of ambient sulfur dioxide (SO_2), nitrogen dioxide (NO_2), ozone (O_3), and PM_{10}. In this study, we use the concentrations of 16 Greater Cairo sites of the EEAA and one of the EMA (Abbasseya) in the period 2010 to 2014. Figure 1 and Table 1S in the supplementary material report all information about these monitoring stations.

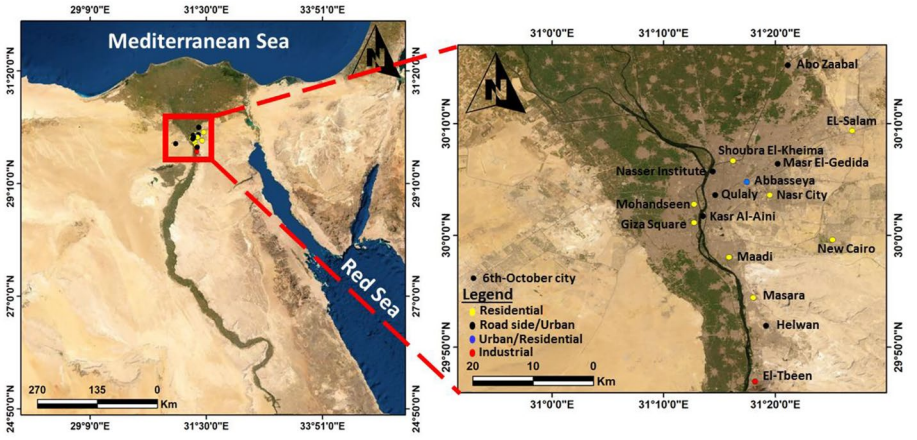

Fig. 1 Map of the 17 stations in Greater Cairo (left) and better resolution map indicating the location of each station within the greater Cairo region (right). The color code indicates the typology of the stations according to the classification of the EEAA and EMA

The recovery rate of the measurements for each year and each station have been evaluated. In terms of number of stations and available data, 2012 shows the highest recovery rate (77% on average). Only the 6th October station had no validated SO_2 and NO_2 data in this year, whereas data from 3 to 4 stations were missing in the other years. Therefore, 2012 was selected for the following analysis. The recovery rates and the number of values exceeding at each site the daily SO_2, NO_2 and PM_{10} limits of the air World Health Organization quality guidelines (WHO 2021, https://www.who.int/news-room/fact-sheets/detail/ambient-(outdoor)-air-quality-and-health) are reported in Table 2S.

At most stations, the levels of PM_{10} always exceed the daily guideline value (45 $\mu g.m^{-3}$), thus confirming the very high PM_{10} loading in Greater Cairo already highlighted in previous studies (Favez et al. 2008a, b; Kanakidou et al. 2011; Wheida et al. 2018; Zakey et al. 2008).

Except at the Masara station, from 3% to 28% of the SO_2 recorded data are higher than recommended by the WHO values (40 $\mu g.m^{-3}$) but the level of exceedance is variable from one station to the other and depends on their typology. For NO_2, the levels remain usually higher than the WHO threshold (25 $\mu g.m^{-3}$) with exceedances ranging from 46% to 99% except at the Shoubra El-Kheima station where only 6% of the recorded data are higher than this limit.

In order to reduce the number of stations retained for the analysis of the effect of dust on trace gas concentrations, we used Agglomerative hierarchical clustering (hereinafter referred to as AHC) to classify the 17 sites into homogeneous groups with similar features. Indeed, AHC is a well-established associativity analysis methodology allowing the identification of the inherent or natural groupings of objects (Johnson and Wicherrn 2007). This multivariate method has come to be recognized as an effective statistical tool to deal with tasks as grouping time series (e.g., Gramsch et al. 2006; Afif et al. 2008; Govender and Sivakumar 2020). In AHC, each pollutant is represented by a matrix of up to 17 columns (one for each station with data in 2012) and a number of rows corresponding to the number of hourly measurements available in the year 2012. For instance, 1589 PM_{10} measurements at 17 sites, 1696 SO_2 measurements at 15 sites, and 4754 NO_2 measurements at 13 sites are available in 2012., we used the XLSTAT 2016 software from AddinSoft to calculate dissimilarities of squared Euclidean distances then Agglomerative Hierarchical Clustering according to Ward (1963).

2.2 Identification and characterization of the dust events

The massive advection of mineral dust produced by wind erosion in the deserts located upwind of Cairo leads to a sharp increase (up to several hundreds of $\mu g.m^{-3}$) of the PM_{10} concentrations recorded at the GC air quality monitoring stations. These events are generally caused by eastbound depressions and are associated with strong west/southwest winds and dry air masses (El-Askary and Kafatos 2008; Eltahan et al. 2018). Therefore, the detection of dust cases will be based primarily on the measurement of unusually large PM_{10} concentrations (i.e., >95th percentile of the yearly measurements) coinciding with back trajectories confirming that the air masses had been travelling above desert areas before reaching GC. These air-mass back trajectories are calculated and plotted with the HYSPLIT model (Stein et al. 2015) using the ZeFir tool under Igor Program (Petit et al. 2017).

In a second step, the observations of the Moderate Resolution Imaging Spectroradiometer (MODIS) aboard the Aqua and Terra spacecraft will be used to confirm the presence of

plumes of mineral dust above GC. These images were downloaded from the NASA website (https://worldview.earthdata.nasa.gov/).

Finally, the inversion of the measurements of the Aeronet Robotics Network (AERONET) sunphotometer (Holben et al. 1998) operated at the Abbasseya station of the EMA allowed characterizing of the aerosol present in the atmospheric column above GC. In this work, we used the quality-assured (level2, version 3) inversion products downloaded from the Aeronet portal (http://aeronet.gsfc.nasa.gov/), and more precisely the Aerosol optical depth (AOD) at wavelength 500 nm, the Angstrom exponent (AE) calculated between 440 and 876 nm, and the Single scattering albedo (SSA) at 440 nm. Although the sunphotometer measurements are not performed in cloudy conditions or at night, which means that its data are not acquired as regularly as those of the air quality network, these products will be precious as inputs to evaluate the photolysis rate ($J\mathrm{NO_2}$) of $\mathrm{NO_2}$ with the Tropospheric Ultraviolet and Visible (TUV) radiation model.

2.3 Meteorological conditions

Hourly averages of various meteorological parameters are recorded at the Abbasseya meteorological station located in the core of GC. The seasonal variability of the dry air temperature (T) and relative humidity (RH) in 2012 does not differ from that of the other years of the 2010 -2014 period (Fig. 1S). T varies between 10 and 40 °C in the transitional seasons but is less variable in winter (9-25 C°) and summer (21-42 C°). On average, RH is particularly low as it does not exceed 60% in all seasons. The prevailing winds have speeds between 6-9 $\mathrm{m.s^{-1}}$ and are from the north/north-east sector (0-45 degrees) (Fig. 2S). However, particularly strong (speed 9-12 $\mathrm{m.s^{-1}}$) south-western winds were recorded in winter (Fig. 2S).

2.4 Comparison of dusty and non-dusty day concentrations

For detecting any potential impact of mineral dust on the $\mathrm{SO_2}$, $\mathrm{NO_2}$, and $\mathrm{O_3}$ concentrations, we compared their concentrations during dust events with those of non-dust periods. However, this comparison only makes sense if the effect of confounding factors has been accounted for. Indeed, the variability of trace gas concentrations is driven by numerous factors such as their direct primary emissions, chemistry, and dilution. Therefore, to detect any potential effect of dust surface on the uptake of reactive trace gas, one should make sure that the comparison with non-dust cases is performed in similar conditions. In the following, we first list the factors that need to be controlled, then present the statistical tests used for the comparison of the dust and non-dust cases. The evaluation of the role of the potential confounding factors will be discussed in the Results section.

2.4.1 Major confounding factors

In urban areas, the emission of primary pollutants or of the precursors of secondary ones usually varies with the hour of the day, the day of the week (weekends or holidays versus business-as-usual days), or the season. In order to minimize the bias introduced by differences in the emissions, we compared the gas concentrations of dust days with those of the same days and hours of the previous and following weeks. In doing so, we implicitly assume that for a given day and hour the emissions do not vary considerably from one week to the other, and thus avoid the risk of comparing a working day with

a none working one, which could have occurred if we had compared the dust day with the previous and the following days.

Meteorology is also expected to affect trace gas variability. Wind speed (U) and the height (H) of the planetary boundary layer (PBL) play an obvious role in the concentrations of the gaseous species because they control their dispersion. The combined effects of U and H are often quantified by the means of the so-called 'Ventilation Index', which is simply equal to their product (Mahmoud et al. 2008). Because the uptake of SO_2 by mineral particles is enhanced by the presence of water on their surface, the influence of potential differences in atmospheric relative humidity between dusty and non-dusty days must also be evaluated. The basic meteorological variables necessary for these quantifications are measured at the EMA's site of Abbasseya (relative humidity, wind direction…) or available (U, H) as products of the ERA5 reanalysis of the European Centre for Medium-Range Weather Forecast (ECMWF). These products were downloaded from https://cds.climate.copernicus.eu/cdsapp#!/dataset/reanalysis-era5-single-levels?tab=form.

Finally, by absorbing and scattering solar radiation the presence of the dust aerosol layer could alter the photolysis frequency of one of the target trace gas, namely NO_2 (JNO_2). Indeed, during a Saharan dust event of the MINATROC campaign in Cape Verde a reduction of 17% was observed for $J(NO_2)$ (De Reus et al. 2005). Therefore, the potential effect of dust on JNO_2 needs to be evaluated. Due to the absence of radiometric $J(NO_2)$ measurements, this effect was quantified by running the on-line TUV model version 5.3 available at https://www.acom.ucar.edu/Models/TUV/Interactive_TUV/. Besides date and time, the input data are latitude, longitude, altitude, surface albedo, the wavelength range of calculation (300-400 nm), and the optical properties of the aerosols (AOD_500 nm, AE_440-870 nm, and SSA_440 nm). Those parameters have been specified for EMA's site of Abbasseya where the AERONET sunphotometer is located.

2.4.2 Statistical comparison of dust days versus non-dust days

The comparison of trace gas concentrations (corrected for the effect of confounding factors as detailed in results section during dust and non-dust days was performed for the stations representative of the clusters identified by the AHC. In order to choose the most appropriate statistical test for this comparison, we first evaluated the normality and lognormality of the distributions by the Shapiro-Wilk test (Shapiro and Wilk 1965). Because the test revealed the absence of normality or lognormality in these distributions, we decided to apply the test of Kruskal-Wallis (KW) (Kruskal and Wallis 1952). Indeed, being a nonparametric method, the Kruskal–Wallis test does not assume a normal distribution of the residuals and can be used to test the equality of medians of a group of independent samples. The null hypothesis is that the medians of the tested group are equal. The alternative hypothesis is obtained when at least one sample is significantly different from the others.

Before performing the comparison with the dust days, the equivalence of the concentrations of the non-dust days used as the reference was checked by a first application of the KW test. The significance was assessed at the 95 % confidence interval: then, if the null hypothesis was confirmed, ($p > 0.05$), the test was applied in a second step to the whole group of non-dust and dust days to check if the dust day was different from the others.

3 Results and discussions

3.1 Agglomerative hierarchical clustering

3.1.1 PM_{10}

The results of the application of AHC to PM_{10} are reported on Fig. 2. The dendrogram (upper panel) shows that the 17 stations are distributed into three clusters of different importance: class 1 (C1, 9 stations), class 2 (C2, 7 stations) and class 3 (C3, only the Qulaly station). The dotted line represents the truncation which led to three homogeneous classes. The stations most representative (the so-called 'central objects') of C1, C2, and C3, are El-Salam, Masara, and Qulaly, respectively. The dissimilarity between C1 and C3 is larger than the one between C2 and C3, which suggests that the levels and the variability of PM_{10} concentrations at Qulaly station resemble more those of the 7 stations of C2 (and particularly Abo Zaabal, which is very close to Qulaly on the dissimilarity scale) than those of the 9 stations of C1.

This clustering is consistent with the different ranges of PM_{10} levels observed at the stations and their three distinct types of diurnal variability (lower panel of Fig. 2). In C1, PM_{10} is the lowest and varies between 73 and 261 $\mu g.m^{-3}$. These -relatively- moderate levels and their lack of clear diurnal variability (Fig. 2) suggest that the C1 stations are not under the direct influence of any specific source of PM and that they can be considered as being representative of the PM_{10} background levels in the GC area. Noteworthy, this could be consistent with the fact that the 9 stations of C1 are not located in the very heart of the GC domain. Three of them are even at its western (6-Oct station) or eastern (El-Salam and New Cairo stations) boundaries. On average, the levels of PM_{10} mass concentrations in C2 (172 to 404 $\mu g.m^{-3}$) are higher than in C1. Of the 7 sites of C2, 4 are located near industrial facilities: namely, Abo Zaabal, Shoubra El-Kheima, Helwan, and El-Tbeen. The 7 sites are distributed along a north (Abo Zaabal) to south (El-Tbeen) axis. As highlighted by (Mostafa et al. 2019), the higher levels of PM_{10} along this axis can be explained in part by the neighboring to near industrial regions but also by the dominant northern wind (Fig. 2S). The diurnal variations of PM_{10} in C2 display two peaks: a well-marked morning peak at 10 AM and an evening peak at 8 PM separated by a drop in the middle of the day. This typical diurnal variability is related to variations in both the anthropogenic activities and boundary layer height.

The Qulaly monitoring station is the only one representing C3. Its PM_{10} diurnal variations are similar to those of C2, but it is distinguished by the AHC because its hourly average levels are considerably larger (268 to 449 $\mu g.m^{-3}$) than in C2 and its mid-afternoon drop is less pronounced.

3.1.2 SO_2

The results of AHC on SO_2 data are shown in Fig. 3. The dendrogram shows that the 15 stations are distributed in four clusters. Two stations are isolated into one single cluster: Qulaly (C4) as for PM_{10} and Abo Zabaal on the North-Eastern border (C2). Both stations show the highest SO_2 levels (19-33 $\mu g.m^{-3}$ and 17-36 $\mu g.m^{-3}$, respectively) but their diurnal variabilities differ. Abou Zabaal displays a bimodal distribution with two well-pronounced morning and evening peaks similar to those of PM_{10} in cluster C2 (Fig. 3), whereas no mid-afternoon drop is observed at Qulaly. C1 (8-28 $\mu g.m^{-3}$) and C3 (13-32 $\mu g.m^{-3}$) contain

7 and 6 stations, respectively. The clustering results cannot be explained by the typology or geographical location of the sites but what is observed is that the variance between stations in C1 is lower than the variance between stations grouped in C3 (Fig. 3).

As for PM_{10}, C1 shows a background-like variability with only a small increase of SO_2 between 06h and 10h local time (morning rush hours). At all other stations, the morning peak is more pronounced. In C2, and to a lesser extent in C3, a second increase of SO_2 is observed between 18h LT and 20h LT. As described by Mostafa et al. (2019), the combustion of sulfur-containing fuels (e.g., oil and diesel) might explain the morning and late evening peak concentrations. Those peaks are enhanced at traffic sites like Qulaly. As for PM_{10}, the drop in the middle of the day is attributed to stronger vertical mixing.

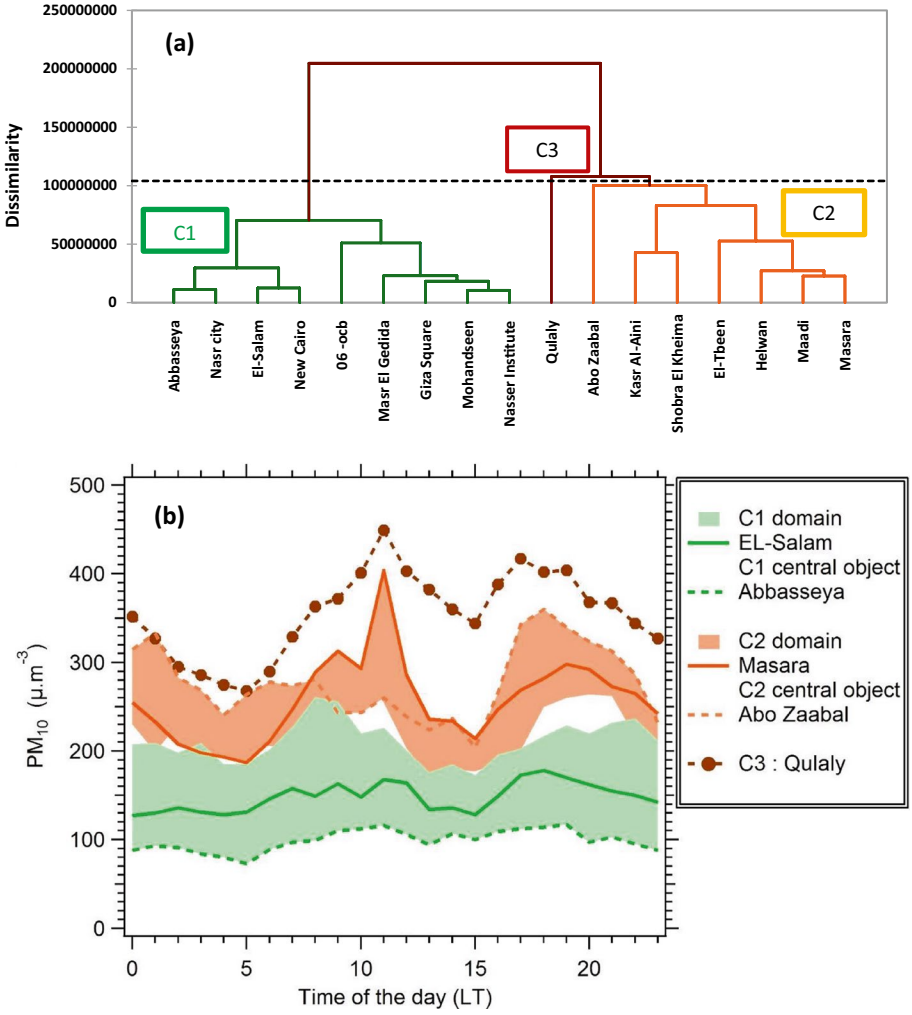

Fig. 2 **a** Dendrogram for PM_{10} data (upper panel, in which the dotted line represents the truncation level) and **b** average diurnal variability of PM_{10} in each cluster and at representative stations (lower panel). Central object represents the object nearest to the centroid in each class

3.1.3 NO_2

The results of AHC on NO_2 data are reported in Fig. 4. Most of the sites (9 out of 13) were grouped into one class (C1), C3 contains 2 stations, C2 corresponds to Abo Zaabal, and C4 to Nasr city where 92% of the data were greater than the WHO hourly limit (Table 2S). The C1 stations show a background-like variability characterized by a smooth increase during the course of the day with a maximum of around 18h LT indicating the secondary production of NO_2. The third cluster (C3) contains Qulaly and Abbasseya where the diurnal variability was the same during night hours and similar during the day but the levels at Qulaly were higher. All sites show a bimodal variability at traffic rush hours (06h to 10h LT and 16h to 20h LT). However, at Nasr City (C4) and Abo Zabaal (C2), the night-time levels of NO_2 are larger than those observed in the afternoon.

In summary, on average and for the year 2012, most of the stations either show a background like or a bimodal variability with concentrations peaking at traffic rush hours. This behavior is observed also for the secondary product NO_2. These commonalities can most probably be explained in part by traffic emissions, which are one driver of the diurnal variability, but the role played by the boundary layer dynamics is also crucial as will be shown below.

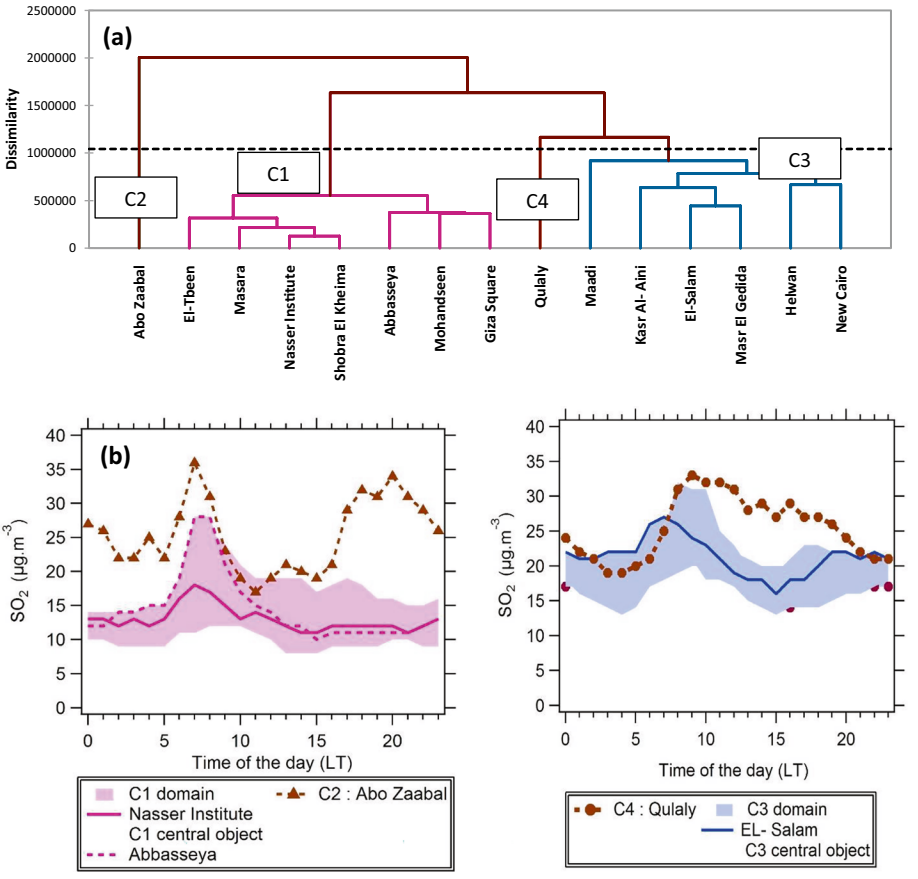

Fig. 3 **a** Dendrogram for SO_2 data (upper panel, in which the dotted line represents the truncation level), and **b** average diurnal variability of SO_2 in each cluster and at representative stations (lower panels)

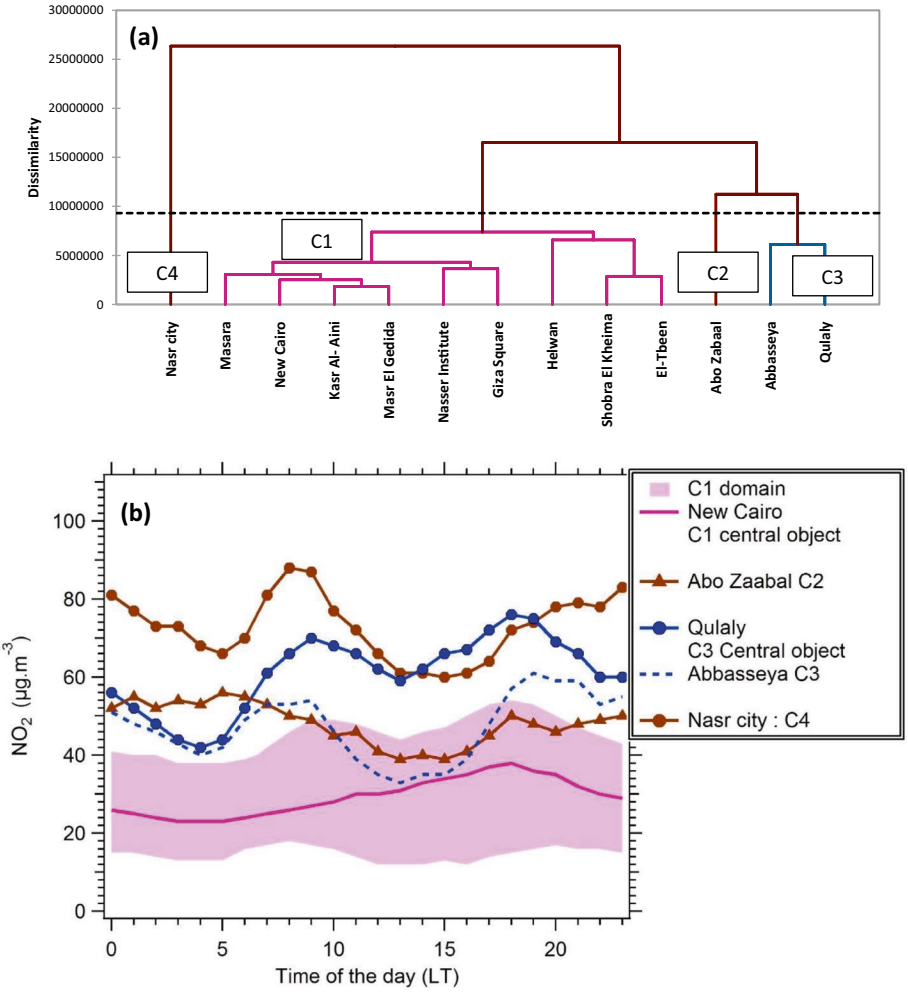

Fig. 4 **a** Dendrogram for NO_2 data (upper panel, in which the dotted line represents the truncation level), and **b** average diurnal variability of NO_2 in each cluster and at representative stations (lower panel)

3.2 Identification of dust events from in-situ and remote sensing observations

As explained in the Methods section, dust events are primarily extracted when PM_{10} exceeds the 95th percentile (446 $\mu g.m^{-3}$) of the measurements performed at all stations. The analysis of air mass trajectories with the ZeFir tool (Petit et al. 2017) based on the HYSPLIT model and the examination of MODIS images are also used to support the dust event selection (Figs. 3S and 4S). The application of this procedure yields seven dust events distributed over eight days (or dust cases) whose details are reported in Table 1 for the three PM_{10} Central Object stations (El-Salam, Masara and Qulaly) extracted by the AHC. Consistent with Eltahan et al. (2018) who noted that dust storms usually occur in winter or spring in GC, four of the 2012 events occurred in wintertime and three in springtime. The air-mass back trajectories and the MODIS images confirm the Saharan origin of dust that came either from the south-western desert of Egypt or from the Libyan Desert.

Table 1 Average concentration of ambient air pollutants during the selected dust cases at the stations representative of the 3 PM_{10} clusters identified by the hierarchical clustering

Case	Date	Start	End	RH	WS	UH	Masara (µg.m^{-3})					EL-Salam (µg.m^{-3})					Qulaly (µg.m^{-3})				
				%	m.s^{-1}	m^2.s^{-1}	PM_{10}			SO_2	NO_2	PM_{10}			SO_2	NO_2	PM_{10}			SO_2	NO_2
1	**Jan-30**	6:00	18:00	60	7	5004	298	±	197	5	45	228	±	236	17	N/A	819	±	653	21	47
2	**Feb-07**	0:00	23:00	38	8	3640	995	±	399	6	37	922	±	540	18	N/A	1481	±	385	21	37
3	**Feb-17**	6:00	15:00	47	12	12195	494	±	117	7	15	498	±	153	12	N/A	968	±	353	23	32
4	**Feb-28**	8:00	18:00	39	12	16194	677	±	295	10	15	654	±	331	21	N/A	1371	±	634	23	38
5	**Apr-01**	10:00	20:00	23	12	17526	977	±	446	11	25	938	±	516	13	N/A	1293	±	637	8	46
6-A	**Apr-18**	6:00	23:00	30	9	7895	1137	±	498	11	37	861	±	498	16	N/A	1540	±	562	9	45
6-B	**Apr-19**	0:00	21:00	37	5	2499	784	±	363	5	23	607	±	235	10	N/A	1193	±	356	10	43
7	**May-22**	20:00	23:00	32	6	917	687	±	248	17	63	617	±	369	19	N/A	705	±	319	11	39

N/A is used for the missed data

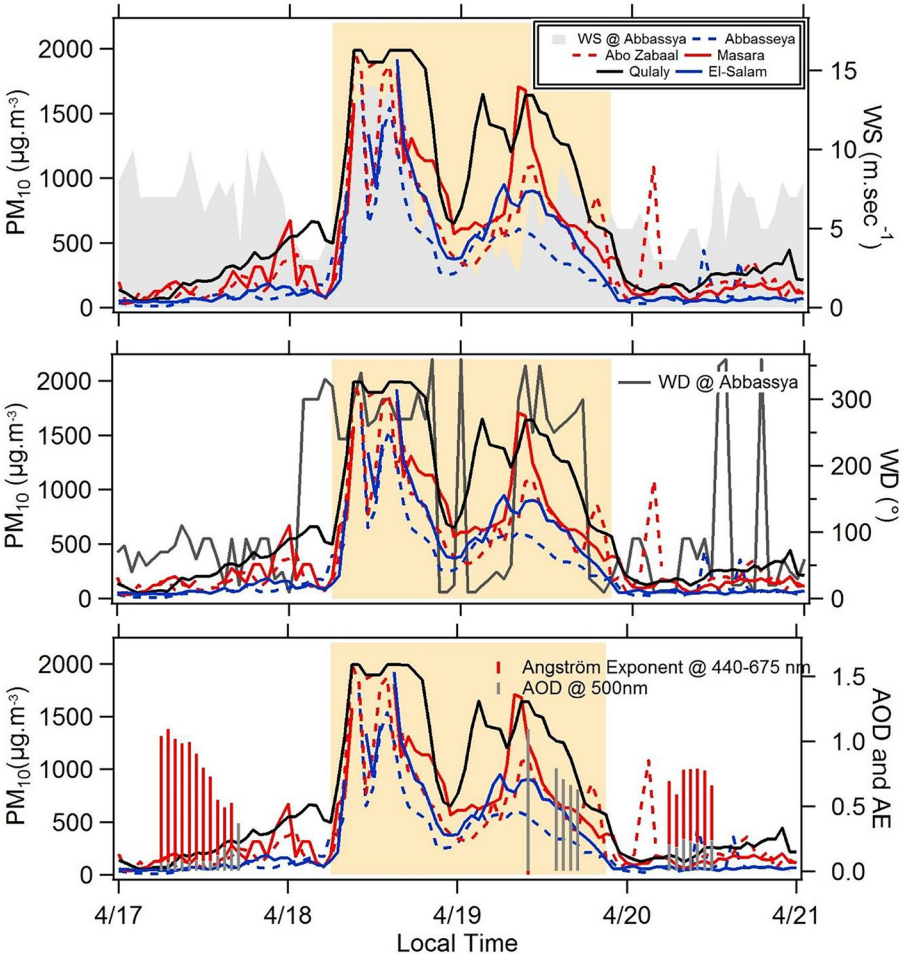

Fig. 5 Example of time series of PM_{10}, wind speed (WS), wind direction (WD), AOD and Ångström coefficient for the Cairo stations representative of the three clusters before, during and after the dust events of 18 and 19 April 2012 (cases 6-A and 6-B in Table 1). The dust event is color-coded in orange

Wintertime dust events were characterized by a larger RH (38-60%) than the springtime (23-37%) ones. Overall, RH is usually lower than 60% and close to 40% on average. The duration of the events ranged from three hours (case 7, at night) to more than one day (case 6, which is therefore split into 6A and 6B in Table 1). In all cases, the largest average PM_{10} are recorded at Qulaly. The average PM_{10} at El-Salam compares to that of Masara. The range of PM_{10} variations is from 228 ± 236 $\mu g.m^{-3}$ at El-Salam (case 1) to 1540 ± 562 $\mu g.m^{-3}$at Qulaly (case 6-A). The available levels of SO_2, NO_2 and O_3 are also reported. During the dust events, the wind speed (WS) can reach 12 $m.s^{-1}$ on average (cases 3, 4 and 5). The largest values of the ventilation index coincide with these strong wind conditions.

Figure 5 illustrates the temporal evolution of the atmospheric conditions before, during, and after the 6-A and 6-B dust cases at a selection of stations including the PM_{10} clustering central object stations. During the two dust events, all stations show a

consistent and remarkable tenfold increase in their PM_{10} loadings. The increase of PM_{10} is correlated with the increase of the wind speed recorded at the Abbasseya station (up to 10 $m.s^{-1}$) and the wind direction shifted to the Western sector a few hours before, pointing out the Saharan desert as the source of dust. The wind direction observed in situ is consistent with the trajectory analysis in the Supplement Material (Fig. 4S). During case 6-B, the AOD and AE values are available and equal to 0.8 and 0.0, respectively. The very low value of the AE, characteristic of coarse particles, confirms the dust-like nature of the aerosol. Outside the dust event, the AOD and AE are below 0.5 and above 0.5, respectively, indicating a rather mixed aerosol (El Metwally et al. 2008).

3.3 Evaluating the diurnal variability of trace gas concentrations

A common and simple approach like the one described in Xie et al. (2005) consists in comparing the absolute concentrations of reactive trace gases before, during and after the dust event in order to test whether a decrease in their concentrations is observed when dust is present. Our purpose here is to illustrate how much this approach is challenging regarding the high temporal (hourly) variability of the reactive trace gases close to anthropogenic emission sources. An example of the hourly variability is illustrated in Fig. 6 for dust event n°5 at the Abbasseya station. The diurnal variability of the hourly

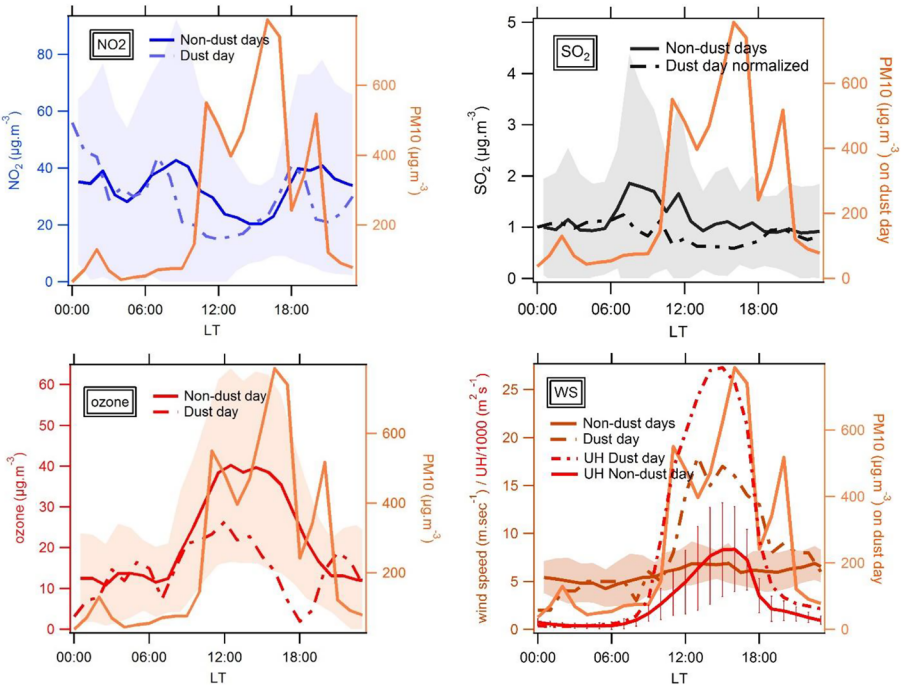

Fig. 6 Diurnal variations of the three trace gases, PM_{10}, wind speed and ventilation index at Abbasseya station in April 2012 during non-dust days and during the dust storm of 1 April 2012 (case 5). The hourly concentrations of SO_2 are relative to the night-time values

SO_2, NO_2 and ozone concentrations for the non-dust days of April 2012 is compared to that of the dust day (April 1st). Note that to facilitate the comparison of days with different levels of SO_2 concentrations, the SO_2 data of Fig. 6 have been normalized to their average night-time values.

The daytime levels of all the trace gases during the dust event of April 1st (dotted lines) tend to be lower than during the non-dust days (solid lines). However, they remain within the limit of one standard deviation (shaded areas), which is quite large. The drop in ozone concentrations is coincident with the sharp increases in the wind speed, ventilation index and PM_{10} levels, but the decrease of the NO_2 and SO_2 concentrations precedes them by 2 to 4 hours, respectively. Therefore, the drop in concentrations cannot be explained only by the ventilation effect or the increase of the PM_{10} concentration. This example illustrates the complex interplay between the various source- and sink-terms governing the diurnal variability. In a nutshell, the important day-to-day and hourly variability of the trace gas concentrations in urban areas makes it difficult to ascribe any clear drop of these concentrations to the advection of dust. In particular, one cannot compare absolute concentrations during the few hours preceding and following the dust storms, as in Xie et al. (2005). In order to minimize the effect of these day-to-day and hourly variations of anthropogenic activities, we assumed that their pattern did not change significantly from one week-day to the same week-days of the same month and therefore decided to compare the dust days with the same non-dust weekdays of the preceding and following weeks.

3.4 Evaluating the potential effect of confounding factors

During an intense dust event, the reduction of the photolysis frequency of NO2 [J(NO2)] due to the absorption and scattering of solar radiation by the dense aerosol layer could also play a role. This role was evaluated for the only dust case (6-B) for which Aeronet aerosol optical properties were available. The comparison with non-dust days (Table 3S) suggests that there should be only a minimal (between 1 and 8%) reduction of the photolysis frequency.

Finally, wind speed tends to be larger during dust events than on non-dust days and this favors the dispersion of the trace gases. The variations of the boundary layer height also have direct implications for their concentrations. In summary, large U associated with large H should lead to lower concentrations of SO_2 and NO_2 than usual conditions. This effect of the ventilation is clearly illustrated by the fact that the largest SO_2 (Fig. 7) and NO_2 (Fig. 5S) concentrations are systematically associated with low ventilation indices. This emphasizes the need to compensate for the role of UH differences in the comparison of the dust days (usually characterized by large UH) and non-dust ones. In the following, we will take this effect into account by weighing (multiplying) the NO_2 and SO_2 concentrations by UH.

3.5 Comparison of trace gas mixing ratios: dust days versus non-dust days

In this section, we explore the effect on the concentrations of reactive trace gases of the high PM_{10} loadings observed in Greater Cairo during dust events. As explained above, these concentrations are weighted by UH to account for the impact of possible differences of ventilation index between the dusty and non-dust days. The comparison between dusty and non-dusty days is performed when the Kruskal-Wallis test previously applied to the group of non-dust days used as a reference confirms their consistency of behavior ($p > 0.05$).

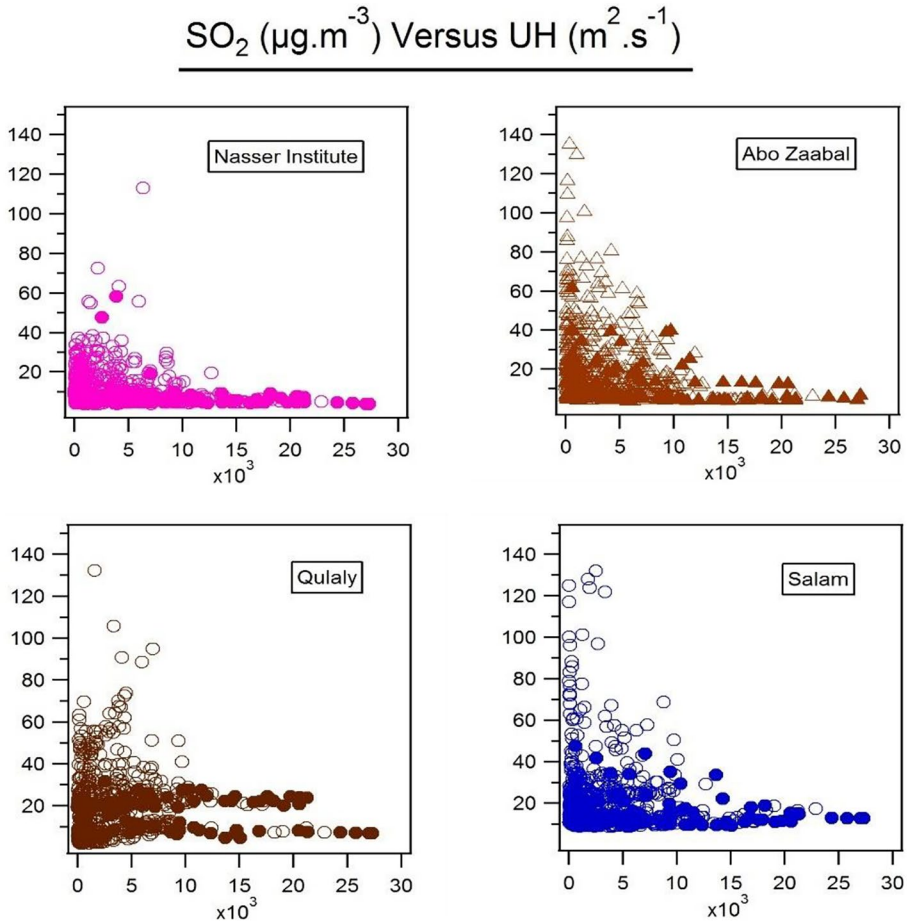

Fig. 7 Scatter plot of SO_2 concentrations vs Ventilation index at the 4 representative stations yielded by the AHC. The color code is the same as on Fig. 3 and the filled (empty) markers correspond to dust (non-dust) periods

3.5.1 Sulfur dioxide

The results of the statistical tests for the stations representative of the four clusters are presented in Table 2. For the eight non-dust groups and the four stations (32 combinations), 15 have p values larger than 0.05 (5, 4, 3, and 3 cases at Nasser Institute, Abo Zabaal, El-El-Salam, and Qulaly stations, respectively). This is an indication that there was no statistical difference between the non-dust days within these groups. On the opposite, the remaining cases (i.e., those for which $p < 0.05$) show statistical differences that reveal their absence of homogeneity. Those cases were therefore not used for the following comparison with the dust days.

After including the dust days in the 15 tested groups, p remains larger than 0.05 in 8 cases, thus showing that the dust days are not different from the non-dust ones. In the 7 other cases (Table 2), the weighted concentrations of SO_2 during these dust events are statistically different from those of the non-dust days but these differences can be due either to an enhancement (5 out of 7) or to a decrease (2 cases) of the weighted SO_2

Table 2 Kruskal-Wallis results for comparing weighted SO_2 concentrations during non-dust days and after adding a dust day to the test at the 4 sites representative of each cluster

	C1				**C2**				**C3**				**C4**			
	UH-weighted SO_2 Nasser Institute				**UH-weighted SO_2 @ Abo Zaabal**				**UH-weighted SO_2 @ EL-Salam**				**UH-weighted SO_2 @ Qulaly**			
	Non dust		**with dust**		**Non dust**		**with dust**		**Non dust**		**with dust**		**Non dust**		**with dust**	
Case	**DF**	**p Value**	**DF**	**p Value**	**DF**	**p Value**	**DF**	**p Value**	**DF**	**p Value**	**DF**	**p Value**	**DF**	**p Value**	**DF**	**p Value**
1	3	0.13	4	0.21	5	0.00	-	-	6	0.13	7	0.21	6	0.00	-	-
2	3	0.00	-	-	3	0.00	-	-	3	0.00	-	-	3	0.00	-	-
3	6	0.23	7	0.14	**6**	**0.16**	**7**	**0.00**	5	0.00	-	-	5	0.03	-	-
4	2	**0.50**	**3**	**0.00**	3	0.00	-	-	3	0.00	-	-	1	0.00	-	-
5	5	**0.40**	**6**	**0.05**	4	0.07	5	0.06	3	0.04	-	-	**5**	**0.17**	**6**	**0.01**
6-A	3	0.00	-	-	3	0.89	4	0.82	2	0.22	3	0.23	**3**	**0.13**	**4**	**0.01**
6-B	3	0.18	4	0.06	**2**	**0.18**	**3**	**0.01**	**3**	**0.06**	**4**	**0.03**	3	0.61	4.00	0.66
7	3	0.02	-	-	2	0.02	-	-	3	0.00	-	-	3	0.02	-	-
Summary	P > 0.05		P < 0.05		P > 0.05		P < 0.05		P > 0.05		P < 0.05		P > 0.05		P < 0.05	
	5		2		4		2		3		1		3		2	

Bold values represent the significant difference after adding a dust day to the test. DF is the degree of freedom of the test = (number of data groups-1)

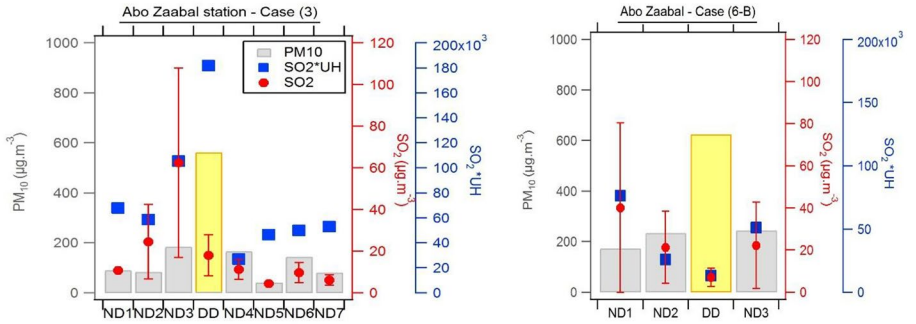

Fig. 8 Examples of comparison between non-dust days (ND) and dust day (DD) at Abo-Zabaal station. Error bars are the standard deviations of SO_2

concentrations during the dust event. Figure 8 provides an example of these contrasting behaviors for the Abo Zaabal station. During event 6B, the absolute SO_2 concentrations (red points) were lower than during the comparable non-dust week-days and they remain so (blue points) after accounting for the effect of ventilation. In the case of event 3, the SO_2 concentrations were similar during the dust and non-dust days, but they become larger after the weighing by UH.

This suggests that the decrease of the SO_2 concentrations observed during some dust events in Cairo is rather due to the increase of the ventilation index (5 cases out of 7) than to uptake at the surface of the dust particles.

Event 6B (Table 2) is particularly interesting in the sense that it allows comparing the potential impact of mineral dust on the SO_2 concentrations at the 4 stations during the same event. After the inclusion of the dust day, the p values yielded by the KW test indicate the absence of effect on the SO_2 concentrations at Nasser Institute and Qulaly ($p>0.05$), but a significant one at (a decrease) at Abo Zaabal and El El-Salam.

3.5.2 Nitrogen dioxide

The same procedure as for SO_2 has been applied to NO_2 and the results of the statistical tests are presented in Table 3. For the 8 groups of non-dust days at the 4 stations, p-values are found to be larger than 0.05 in 15 cases (3, 2, 5, and 5 cases for New Cairo, Abo Zaabal, Qulaly, and Nasr City, respectively).

After inclusion of the dust days in the 15 tested groups, the resulting p values remain larger than 0.05 in 9 cases. In the other 6 cases (Table 3), p value is < 0.05 in 1, 1, 3, and 1 occurrence at the four stations, respectively. A reduction (by 48%) of the UH-weighted NO_2 is only observed at the Qulaly station during case 7 (Fig. 9). In the 5 remaining cases, the difference with the non-dust days is due to an enhancement of the NO_2 concentration and not to a reduction.

3.5.3 Ozone

The statistical tests could be applied for three of the dust events and only at Abbasseya, which is the only station where the ozone concentration was measured. The non-dust day p-value is larger than 0.05 only during events 5 and 6B. After inclusion of the dust day in this group, the p value

Table 3 Kruskal-Wallis results for comparing normalized NO_2 concentrations during non-dust days and after adding a dust day to the test at the selected sites

	C1				**C2**				**C3**				**C4**			
	UH-weighted NO_2 @ New Cairo				**UH-weighted NO_2 @Abo Zaabal**				**UH-weighted NO_2 @ Qulaly**				**UH-weighted NO_2 @ Nasr City**			
	Non dust		**With dust**		**Non dust**		**With dust**		**Non dust**		**With dust**		**Non dust**		**With dust**	
Case	**DF**	**p Value**	**DF**	**p Value**	**DF**	**p Value**	**DF**	**p Value**	**DF**	**p Value**	**DF**	**p Value**	**DF**	**p Value**	**DF**	**p Value**
1	6	0.06	7	0.08	**4**	**0.06**	**5**	**0.04**	6	0.02	-	-	2	0.08	N/A	N/A
2	3	0.00	-	-	3	0.00	-	-	3	0.00	-	-	1	0.00	-	-
3	5	0.00	-	-	2	0.00	-	-	**5**	**0.06**	**6**	**0.00**	**4**	**0.22**	**5**	**0.01**
4	2	0.02	-	-	-	-	-	-	2	0.00	-	-	2	0.02	-	-
5	2	0.04	-	-	3	0.03	-	-	**5**	**0.16**	**6**	**0.00**	3	0.03	-	-
6-A	**3**	**0.20**	**4**	**0.01**	3	0.00	-	-	3	0.63	4	0.07	1	0.39	N/A	N/A
6-B	3	0.58	4	0.69	1	0.14	2	0.37	3	0.14	4	0.17	1	0.25	N/A	N/A
7	3	0.03			3	0.02	-	-	**3**	**0.12**	**4**	**0.02**	2	0.86	3	0.96
Summary	P > 0.05		P < 0.05		P > 0.05		P < 0.05		P > 0.05		P < 0.05		P > 0.05		P < 0.05	
	3		1		2		1		5		3		2		1	

Bold values represent the significant difference after adding a dust day to the test. N/A represents the missing of data

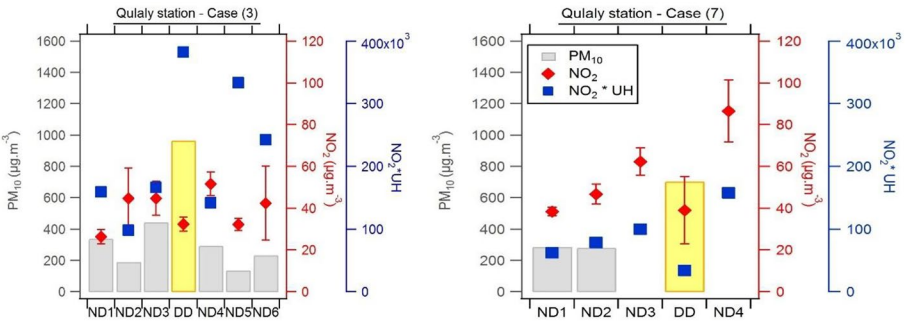

Fig. 9 Examples of comparison between non-dust days (ND) and dust day (DD) at Qulaly station. Error bars are the standard deviations of NO_2

remains larger than 0.05, indicating that there is no significant effect of the presence of mineral dust on the ozone concentration corrected for the effect of the ventilation index (Table 4).

3.6 Discussion

In 2012, eight dust cases were identified and for SO_2, as well as for NO_2, the 17 stations of the air quality monitoring network can be sorted into four representative clusters. Therefore, there is theoretically a maximum of 32 (4 by 8) combinations to test the impact of the presence of dust on the trace gas concentrations by comparison with non-dusty days. Practically, after accounting for the missing data and eliminating the situations for which the behavior of the group of non-dust days was not homogenous enough to serve as a sure-proof reference, this number was reduced to 15 for both SO_2 and NO_2. In slightly more than 50% of the situations (8 and 9 cases, respectively), there was no statistically significant difference in UH-weighted concentrations between the dust and non-dust periods. In the other cases, the majority (5/7 for SO_2 and 5/6 for NO_2) of the observed differences were not due to a reduction of the trace gas concentrations but to an increase. For ozone, the number of usable test-cases is quite limited (only 2), but in both cases, no modification of the UH-corrected concentration is observed in the presence of dust. These results obtained in natural conditions during intense dust events seem to contradict the current assumption mostly based on laboratory observations that heterogeneous reactions at the surface of dust particles act as a significant sink for reactive trace gases.

One first possible explanation for this apparent contradiction lies in the low atmospheric relative humidity prevailing during the dust events in Greater Cairo. Zhang et al. (2019) showed that the uptake of SO_2 on dust particles was facilitated by the presence of NO_2 and

Table 4 Kruskal-Wallis results for comparing normalized O_3 concentrations during non-dust days and after adding a dust day to the test at Abbasseya site

	UH Normalized ozone @ Abbasseya			
	Non dust		with dust	
Case	**DF**	**p Value**	**DF**	**P Value**
5	3	0.23	4	0.18
6-A	1	0.02	--	--
6-B	2	0.07	3	0.16

NH_3 and increase of RH above a threshold of about 50% that was barely reached in Cairo during the dust events of this study. In such conditions of dryness, reactions in the aqueous phase are not possible or at least too limited to induce a detectable reduction of the concentrations of the trace gases. However, a systematic study involving more dust cases and, if possible, a larger range of RH conditions would be necessary to confirm this hypothesis.

4 Summary and conclusion

Greater Cairo is a natural laboratory for studying the interactions between reactive trace gases of anthropic origins and mineral dust produced by wind erosion of the deserts surrounding the megacity. In this work, eightintense dust events of 2012 have been identified and selected as case studies to evaluate the impact of the presence of dust on the concentrations of SO_2, NO_2, and ozone measured at a selection of stations (four for SO_2 and NO_2, one for O_3) representative of the Greater Cairo area. As compared to those of the preceding and following non-dust periods of similar anthropogenic activities, these concentrations are significantly lower during the dust periods. However, our analysis of the role of potential confounding factors (wind speed, boundary layer height, relative humidity, modification of the actinic flux) showed that this drop of the concentrations was a consequence of the larger wind speed and higher boundary layer height prevailing during the dust events and favouring the dispersion of the trace gases. Once this effect is corrected, the application of the non-parametric Kruskal-Wallis test no longer reveals any difference between the dust periods and non-dust reference ones in 8/15, 9/15, and 2/2 cases for SO_2, NO_2, and O_3, respectively. When a statistically significant difference is found, which is due to a decrease of the SO_2 or NO_2 concentrations in only 2/15 and 1/15 cases and to an increase in 5/15 cases (for both gases). These results show that, in Greater Cairo, there is no detectable effect of adsorption of the reactive gases on the surface of the air-suspended dust particles which are contradictory to laboratory experiments indicating this adsorption. They can be primarily interpreted by the relatively low RH (<60%) prevailing in Greater Cairo, particularly during the episodes of Saharan dust advection, the uptake coefficients of the trace gases are expected to be very low.

Supplementary Information The online version contains supplementary material available at https://doi.org/10.1007/s10874-023-09449-4.

Acknowledgments This work is a contribution to the POL-Cair project (# ID 27758) funded by the Science and Technology Development Fund (STDF), Institut de Recherche pour le Développement (IRD) and Agence Universitaire de la Francophonie (AUF). Also, is a contribution to the AQUACHE project (# ID 46269NK) in the frame of IMHOTEP program funded by the Science and Technology Development Fund (STDF), Institut Français d'Egypte (Cairo, Egypt). The authors wish to thank the Egyptian Environmental Affairs Agency (EEAA) and the Egyptian Meteorological Authority (EMA) for providing the data used in this study.

Authors contributions Mohamed Boraiy and Agnes Borbon wrote the manuscript and analysed the data. Ali Wheida and Mostafa El-Nazer collected the data and performed the quality check. Mossad El-Metwally and Fatma El-Sanabary revised the analysis. Salwa Kamal validated the results. Stephane Alfaro and Magdy Abdel Wahab Writing- Reviewing and Editing.

Funding Open access funding provided by The Science, Technology & Innovation Funding Authority (STDF) in cooperation with The Egyptian Knowledge Bank (EKB). This research was supported by Science and Technology Development Fund (STDF), Institut de Recherche pour le Développement (IRD), Agence Universitaire de la Francophonie (AUF) and Institut Français d'Egypte (Cairo, Egypt).

Data availability The datasets analyzed during the current study are available from the corresponding author on reasonable request.

Declarations

Ethical Responsibilities of Authors All authors have read, understood, and have complied as applicable with the statement on "Ethical responsibilities of Authors" as found in the Instructions for Authors and are aware that with minor exceptions, no changes can be made to authorship once the paper is submitted.

Consent to participate Not applicable.

Consent for publication Not applicable.

Conflict of interest The authors declare no competing interests.

References

Abu-Allaban, M., Lowenthal, D.H., Gertler, A.W., Labib, M.: Sources of PM10 and PM2. 5 in Cairo's ambient air. Environ. Monit. Assess. **133**(1), 417–425 (2007). https://doi.org/10.1007/s10661-006-9596-8

Abu-Allaban, M., Lowenthal, D.H., Gertler, A.W., Labib, M.: Sources of volatile organic compounds in Cairo's ambient air. Environ. Monit. Asses. **157**(1), 179–189 (2009). https://doi.org/10.1007/s10661-008-0526-9

Abu-Allaban, Mahmoud, Gertler, A.W., Lowenthal, D.H.: A preliminary apportionment of the sources of ambient PM10, PM2. 5, and VOCs in Cairo. Atmos. Environ. **36**(35), 5549–5557 (2002). https://doi.org/10.1016/S1352-2310(02)00662-3

Afif, C., Chélala, C., Borbon, A., Abboud, M., Adjizian-Gérard, J., Farah, W., et al.: SO2 in Beirut: air quality implication and effects of local emissions and long-range transport. Air Qual. Atmos. Health **1**(3), 167–178 (2008). https://doi.org/10.1007/s11869-008-0022-y

Bian, H., Zender, C.S.: Mineral dust and global tropospheric chemistry: Relative roles of photolysis and heterogeneous uptake. J. Geophys. Res. Atmos. **108**(D21) (2003). https://doi.org/10.1029/2002JD003143

De Reus, M., Fischer, H., Sander, R., Gros, V., Kormann, R., Salisbury, G., et al.: Observations and model calculations of trace gas scavenging in a dense Saharan dust plume during MINATROC. Atmos. Chem. Phys. **5**(7), 1787–1803 (2005). https://doi.org/10.5194/acp-5-1787-2005,2005

Dentener, F.J., Carmichael, G.R., Zhang, Y., Lelieveld, J., Crutzen, P.J.: Role of mineral aerosol as a reactive surface in the global troposphere. J. Geophys. Res. Atmos. **101**(D17), 22869–22889 (1996). https://doi.org/10.1029/96JD01818

El-Askary, H., Kafatos, M.: Dust storm and black cloud influence on aerosol optical properties over Cairo and the Greater Delta region, Egypt. Int. J. Remote Sens. **29**(24), 7199–7211 (2008). https://doi.org/10.1080/01431160802144179

El-Dars, F.M.S., Mohamed, A.M.F., Aly, H.A.T.: Monitoring ambient sulfur dioxide levels at some residential environments in the Greater Cairo Urban Region - Egypt. Environ. Monit. Assess. **95**(1–3) (2004). https://doi.org/10.1023/B:EMAS.0000029908.56178.5a

El-Metwally, M., Alfaro, S. C., Abdel Wahab, M., Chatenet, B.: Aerosol characteristics over urban Cairo: Seasonal variations as retrieved from Sun photometer measurements. J. Geophys. Res. Atmos. **113**(D14) (2008). https://doi.org/10.1029/2008JD009834

El-Metwally, M., Alfaro, S.C., Wahab, M.M.A., Favez, O., Mohamed, Z., Chatenet, B.: Aerosol properties and associated radiative effects over Cairo (Egypt). Atmos. Res. **99**(2), 263–276 (2011). https://doi.org/10.1016/j.atmosres.2010.10.017

Eltahan, M., Shokr, M., Sherif, A.O.: Simulation of severe dust events over Egypt using tuned dust schemes in weather research forecast (WRF-Chem). Atmosphere **9**(7), 246 (2018). https://doi.org/10.3390/atmos9070246

Favez, O., Cachier, H., Sciare, J., Alfaro, S.C., El-Araby, T.M., Harhash, M.A., Abdelwahab, M.M.: Seasonality of major aerosol species and their transformations in Cairo megacity. Atmos. Environ. **42**(7), 1503–1516 (2008a). https://doi.org/10.1016/j.atmosenv.2007.10.081

Favez, O., Sciare, J., Cachier, H., Alfaro, S. C., Abdelwahab, M.M.: Significant formation of water-insoluble secondary organic aerosols in semi-arid urban environment. Geophys. Res. Lett. **35**(15), (2008b).https://doi.org/10.1029/2008GL034446

Goodman, A.L., Underwood, G.M., Grassian, V.H.: A laboratory study of the heterogeneous reaction of nitric acid on calcium carbonate particles. J. Geophys. Res. Atmos. **105**(D23), 29053–29064 (2000). https://doi.org/10.1029/2000JD900396

Govender, P., Sivakumar, V.: Application of k-means and hierarchical clustering techniques for analysis of air pollution: A review (1980–2019). Atmos. Pollut. Res. **11**(1), 40–56 (2020). https://doi.org/10.1016/j.apr.2019.09.009

Gramsch, E., Cereceda-Balic, F., Oyola, P., Von Baer, D.: Examination of pollution trends in Santiago de Chile with cluster analysis of PM10 and ozone data. Atmos. Environ. **40**(28), 5464–5475 (2006). https://doi.org/10.1016/j.atmosenv.2006.03.062

Hassan, S.K.: Sources and cancer risk of heavy metals in total suspended particulate in some square areas of Greater Cairo. Egypt. Indian J. Environ. Protect. (IJEP) **38**(12), 1040–1050 (2018a)

Hassan, S.K., El-Abssawy, A.A., Khoder, M.I.: Effect of Seasonal Variation on the Levels and Behaviours of Formaldehyde in the Atmosphere of a Suburban Area in Cairo, Egypt. Asian J. Atmos. Environ. (AJAE) **12**(4), (2018b). https://doi.org/10.5572/ajae.2018.12.4.356

Hassan, S.K.: Particle-bound polycyclic aromatic hydrocarbon in the atmosphere of heavy traffic areas in Greater Cairo, Egypt: Status, Source, and Human Health Risk Assessment. Atmosphere **9**(10), 368 (2018). https://doi.org/10.3390/atmos9100368

Hassan, S.K., Khoder, M.I.: Chemical characteristics of atmospheric PM2. 5 loads during air pollution episodes in Giza, Egypt. Atmos. Environ. **150**, 346–355 (2017). https://doi.org/10.1016/j.atmosenv.2016.11.026

He, H., Wang, Y., Ma, Q., Ma, J., Chu, B., Ji, D., et al.: Mineral dust and NOx promote the conversion of SO2 to sulfate in heavy pollution days. Sci. Rep. **4**(1), 1–6 (2014). https://doi.org/10.1038/srep04172

Hereher, M., Eissa, R., Alqasemi, A., El Kenawy, A.M.: Assessment of air pollution at Greater Cairo in relation to the spatial variability of surface urban heat island. Environ. Sci. Pollut. Res. 1–14 (2021). https://doi.org/10.1007/s11356-021-17383-9

Holben, B.N., Eck, T.F., Slutsker, I., al, Tanre, D., Buis, J. P., Setzer, A., et al.: AERONET—A federated instrument network and data archive for aerosol characterization. Remote Sens. Environ. **66**(1), 1–16 (1998)

Johnson, R.A., Wichern, D. W.: Applied multivariate statistical analysis. Pearson Prentice Hall (2007). https://doi.org/10.4236/jwarp.2010.26066

Kanakidou, M., Mihalopoulos, N., Kindap, T., Im, U., Vrekoussis, M., Gerasopoulos, E., et al.: Megacities as hot spots of air pollution in the East Mediterranean. Atmos. Environ. **45**(6), 1223–1235 (2011). https://doi.org/10.1016/j.atmosenv.2010.11.048

Knippertz, P., Evans, M.J., Field, P.R., Fink, A.H., Liousse, C., Marsham, J.H.: The possible role of local air pollution in climate change in West Africa. Nat. Clim. Change (2015). https://doi.org/10.1038/nclimate2727

Kruskal, W.H., Wallis, W.A.: Use of ranks in one-criterion variance analysis. J. Am. Stat. Assoc. **47**(260), 583–621 (1952)

Mahmoud, K.F., Alfaro, S.C., Favez, O., Wahab, M.M.A., Sciare, J.: Origin of black carbon concentration peaks in Cairo (Egypt). Atmos. Res. **89**(1–2), 161–169 (2008). https://doi.org/10.1016/j.atmosres.2008.01.004

Marchetti, S., Hassan, S.K., Shetaya, W.H., El-Mekawy, A., Mohamed, E.F., Mohammed, A.M. F., et al.: Seasonal variation in the biological effects of PM2. 5 from greater cairo. Int. J. Mol. Sci. **20**(20), 4970 (2019). https://doi.org/10.3390/ijms20204970

Michel, A.E., Usher, C.R., Grassian, V.H.: Heterogeneous and catalytic uptake of ozone on mineral oxides and dusts: A Knudsen cell investigation. Geophys. Res. Lett. **29**(14), 10–14 (2002). https://doi.org/10.1029/2002GL014896

Mostafa, A.N., Zakey, A.S., Alfaro, S.C., Wheida, A.A., Monem, S.A., Abdul Wahab, M.M.: Validation of RegCM-CHEM4 model by comparison with surface measurements in the Greater Cairo (Egypt) megacity. Environ. Sci. Pollut. Res. **26**(23), 23524–23541 (2019). https://doi.org/10.1007/s11356-019-05370-0

Ndour, N.Y.B., Baudoin, E., Guissé, A., Seck, M., Khouma, M., Brauman, A.: Impact of irrigation water quality on soil nitrifying and total bacterial communities. Biol. Fertil. Soils **44**(5), 797–803 (2008). https://doi.org/10.1007/s00374-008-0285-3

Petit, J.-E., Favez, O., Albinet, A., Canonaco, F.: A user-friendly tool for comprehensive evaluation of the geographical origins of atmospheric pollution: Wind and trajectory analyses. Environ. Model. Softw. **88**, 183–187 (2017). https://doi.org/10.1016/j.envsoft.2016.11.022

Salameh, T., Borbon, A., Afif, C., Sauvage, S., Leonardis, T., Gaimoz, C., Locoge, N.: Composition of gaseous organic carbon during ECOCEM in Beirut, Lebanon: New observational constraints for VOC anthropogenic emission evaluation in the Middle East. Atmos. Chem. Phys. **17**(1), (2017). https://doi.org/10.5194/acp-17-193-2017

Shaltout, A.A., Boman, J., Hassan, S.K., Abozied, A.M., Al-Ashkar, E.A., Abd-Elkader, O.H., et al.: Elemental composition of PM2. 5 aerosols in a residential–industrial area of a Mediterranean Megacity. Arch. Environ. Contam. Toxicol. **78**(1), 68–78 (2020). https://doi.org/10.1007/s00244-019-00688-9

Shaltout, A.A., Hassan, S.K., Alomairy, S.E., Manousakas, M., Karydas, A.G., Eleftheriadis, K.: Correlation between inorganic pollutants in the suspended particulate matter (SPM) and fine particulate matter (PM2. 5) collected from industrial and residential areas in Greater Cairo, Egypt. Air Qual. Atmos. Health **12**(2), 241–250 (2019). https://doi.org/10.1007/s11869-018-0645-6

Shaltout, A.A., Hassan, S.K., Karydas, A.G., Harfouche, M., Abd-Elkader, O.H., Kregsamer, P., et al.: EDXRF analysis of suspended particulate matter (SPM) from residential and industrial areas in Cairo, Egypt. X-Ray Spectrom. **47**(3), 223–230 (2018a). https://doi.org/10.1002/xrs.2830

Shaltout, A.A., Hassan, S.K., Karydas, A.G., Zaki, Z.I., Mostafa, N.Y., Kregsamer, P., et al.: Comparative elemental analysis of fine particulate matter (PM2. 5) from industrial and residential areas in Greater Cairo-Egypt by means of a multi-secondary target energy dispersive X-ray fluorescence spectrometer. Spectrochim. Acta Part B Atom. Spectrosc. **145**, 29–35 (2018b). https://doi.org/10.1016/j.sab.2018.04.003

Shapiro, S.S., Wilk, M.B.: An analysis of variance test for normality (complete samples). Biometrika **52**(3/4), 591–611 (1965)

Stein, A.F., Draxler, R.R., Rolph, G.D., Stunder, B.J.: B., cohen, md, and ngan, f.: Noaa's hysplit atmospheric transport and dispersion modeling system, b. Am. Meteorol. Soc **96**, 2059–2077 (2015). https://doi.org/10.1175/BAMS-D-14-00110.1

Talaat, H., Xu, J., Hatzopoulou, M., Abdelgawad, H.: Mobile monitoring and spatial prediction of black carbon in Cairo, Egypt. Environ. Monit. Assess. **193**(9), (2021. https://doi.org/10.1007/s10661-021-09351-0

Thera, B., Dominutti, P., Colomb, A., Michoud, V., Doussin, J.F., Beekmann, M., Borbon, A.: O 3–NO y photochemistry in boundary layer polluted plumes: insights from the MEGAPOLI (Paris), ChArMEx/SAFMED (North West Mediterranean) and DACCIWA (southern West Africa) aircraft campaigns. Environ. Sci. Atmos. (2022). https://doi.org/10.1039/D1EA00093D

Underwood, G.M., Song, C.H., Phadnis, M., Carmichael, G.R., Grassian, V.H.: Heterogeneous reactions of NO2 and HNO3 on oxides and mineral dust: A combined laboratory and modeling study. J. Geophys. Res. Atmos. **106**(D16), 18055–18066 (2001). https://doi.org/10.1029/2000JD900552

Usher, C.R., Michel, A.E., Grassian, V.H.: Reactions on mineral dust. Chem. Rev. **103**(12), 4883–4940 (2003). https://doi.org/10.1021/cr020657y

Wang, K., Zhang, Y., Nenes, A., Fountoukis, C.: Implementation of dust emission and chemistry into the Community Multiscale Air Quality modeling system and initial application to an Asian dust storm episode. Atmos. Chem. Phys. **12**(21), (2012). https://doi.org/10.5194/acp-12-10209-2012

Ward, J.H., Jr.: Hierarchical grouping to optimize an objective function. J. Am. Stat. Assoc. **58**(301), 236–244 (1963). https://doi.org/10.1080/01621459.1963.10500845

Wheida, A., Nasser, A., El Nazer, M., Borbon, A., El Ata, G.A.A., Wahab, M.A., Alfaro, S.C.: Tackling the mortality from long-term exposure to outdoor air pollution in megacities: Lessons from the Greater Cairo case study. Environ. Res. **160**, 223–231 (2018). https://doi.org/10.1016/j.envres.2017.09.028

World Health Organization (WHO).: Global air quality guidelines: particulate matter (PM2.5 and PM10), ozone, nitrogen dioxide, sulfur dioxide and carbon monoxide: executive summary. (2021). https://www.who.int/publications/i/item/9789240034228

Xie, S., Yu, T., Zhang, Y., Zeng, L., Qi, L., Tang, X.: Characteristics of PM10, SO2, NOx and O3 in ambient air during the dust storm period in Beijing. Sci. Total Environ. **345**(1–3), 153–164 (2005). https://doi.org/10.1016/j.scitotenv.2004.10.013

Zakey, A.S., Abdel-Wahab, M.M., PETTERSSON, J. B. C., Gatari, M. J., & Hallquist, M.: Seasonal and spatial variation of atmospheric particulate matter in a developing megacity, the Greater Cairo, Egypt. Atmosfera **21**(2), 171–189 (2008)

Zhang, S., Xing, J., Sarwar, G., Ge, Y., He, H., Duan, F., et al.: Parameterization of heterogeneous reaction of SO2 to sulfate on dust with coexistence of NH3 and NO2 under different humidity conditions. Atmos. Environ. **208**, 133–140 (2019). https://doi.org/10.1016/j.atmosenv.2019.04.004

Zhang, Y., Carmichael, G.R.: The role of mineral aerosol in tropospheric chemistry in East Asia—A model study. J. Appl. Meteorol. **38**(3), 353–366 (1999). https://doi.org/10.1175/1520-0450(1999)038<0353:TROMAI>2.0.CO;2

Authors and Affiliations

Mohamed Boraiy[1] · Mossad El-Metwally[2] · Ali Wheida[3] · Mostafa El Nazer[3] · Salwa K. Hassan[4] · Fatma F. El-Sanabary[1] · Stéphane C. Alfaro[5] · Magdy Abdelwahab[6] · Agnès Borbon[7]

✉ Mohamed Boraiy
mohmed.mahmoud@eng.psu.edu.eg

[1] Physics and Mathematical Engineering Department, Faculty of Engineering, Port Said University, Port Said, Egypt

[2] Physics Department, Faculty of Science, Port Said University, Port Said, Egypt

[3] Theoretical Physics Department, Physics Institute, National Research Centre, El Behooth Str., Giza 12622 Dokki, Egypt

[4] Air Pollution Research Department, Environment and Climate Change Research Institute, National, Research Centre, El Behooth Str., Giza 12622 Dokki, Egypt

[5] Univ de Paris Est Creteil and Universite Paris Cite, CNRS, LISA F-94010 Créteil, France

[6] Astronomy and Meteorology Department, Faculty of Science, Cairo University, Cairo, Egypt

[7] Laboratoire de Météorologie Physique, UMR6016, Université Clermont Auvergne, OPGC, CNRS, 63000 Clermont-Ferrand, France